International Journal of Fluid Machinery and Systems
Vol. 1, No. 1, October-December 2008

Original Paper

Variable Geometry Mixed Flow Turbine for Turbochargers: An Experimental Study

Srithar Rajoo[1] and Ricardo Martinez-Botas[2]

[1]Faculty of Mechanical Engineering, Universiti Teknologi Malaysia
81310 Skudai Johor, Malaysia
[2]Department of Mechanical Engineering, Imperial College London
SW7 2AZ Exhibition Road, London, United Kingdom

Abstract

This paper investigates a variable geometry (VG) mixed flow turbine with a novel, purposely designed pivoting nozzle vane ring. The nozzle vane ring was matched to the 3-dimensional aspect of the mixed flow rotor leading edge with lean stacking. It was found that for a nozzle vane ring in a volute, the vane surface pressure is highly affected by the flow in the volute rather than the adjacent vane surface interactions, especially at closer nozzle positions. The performance of the VG mixed flow turbine has been evaluated experimentally in steady and unsteady flow conditions. The VG mixed flow turbine shows higher peak efficiency and swallowing capacity at various vane angle settings compared to an equivalent nozzleless turbine. Comparison with an equivalent straight vane arrangement shows a higher swallowing capacity but similar efficiencies. The VG turbine unsteady performance was found to deviate substantially from the quasi-steady assumption compared to a nozzleless turbine. This is more evident in the higher vane angle settings (smaller nozzle passage), where there are high possibility of choking during a pulse cycle. The presented steady and unsteady results are expected to be beneficial in the design of variable geometry turbochargers, especially the ones with a mixed flow turbine.

Keywords : variable geometry turbocharger, mixed flow turbine, steady flow and pulsating flow

1. Introduction

Automotive turbochargers almost in their entirety are equipped with radial turbines, due to the efficiency superiority of a radial design in small geometries. A radial turbine with radial inflow rotor are in most cases designed with zero inlet blade angle (with respect to radial direction), for purpose of maintaining its radial fibre. A mixed flow rotor with its leading edge swept radially downwards, provides an extra degree of freedom to the designer compared to a radial inflow rotor, hence a non-zero inlet blade angle can be achieved while maintaining its radial fibre. Research has shown a substantial amount of exhaust gas energy to be available at velocity ratios of less than 0.7 – the point of highest energy recovery for a conventional radial turbine. For the past three decades research has been carried out to explore the benefits of the mixed flow turbine in terms of lower velocity ratio operation and higher swallowing capacity [1,2,3,4]. For a non-zero rotor blade angle, the peak turbine efficiency point moves to a higher expansion ratio. This is advantageous in a turbocharger application, which is subjected to pulsating flow from the reciprocating engine, where the greater energy of the flow is contained at high pressures.

VGTs have been widely based on radial turbines, particularly in automotive application. Mixed flow turbines with lower inertial characteristic, coupled with variable geometry operation have the capability of enhancing the existing versions of VGTs. Unfortunately, there are not many VGTs which uses mixed flow turbines, and for the very few which exist [5], the nozzle vane used is adapted from radial turbines, these are invariably straight vanes. Due to the non-radial inlet of the mixed flow turbine, the use of straight vanes creates a non-uniform inter-space between the nozzle vane ring and the rotor (viewed from meridional projection). The objective of this work is to study an alternative nozzle vane design and its implication on a mixed flow turbine performance.

Most available published work on VGT is still based on steady-state data. It has been shown in the past research that a turbine's performance during pulsating flow departs from the quasi-steady assumption [3,4,6,7], however most of these work were based on nozzleless turbines. Thus the instantaneous performance evaluation of a VGT in pulsating flow conditions is beneficial in order to better understand its characteristics at different nozzle vane positions. These are presented in the current paper with the

Received July 29 2008; revised November 16 2008; accepted for publication November 17 2008: Review conducted by Prof. Yulin Wu. (Paper number O08020)
Corresponding author: Ricardo Martinez-Botas, Reader in Turbomachinery, r.botas@imperial.ac.uk; work submitted while at CMT Motores Termicos, Universidad Politecnica de Valencia (Spain)

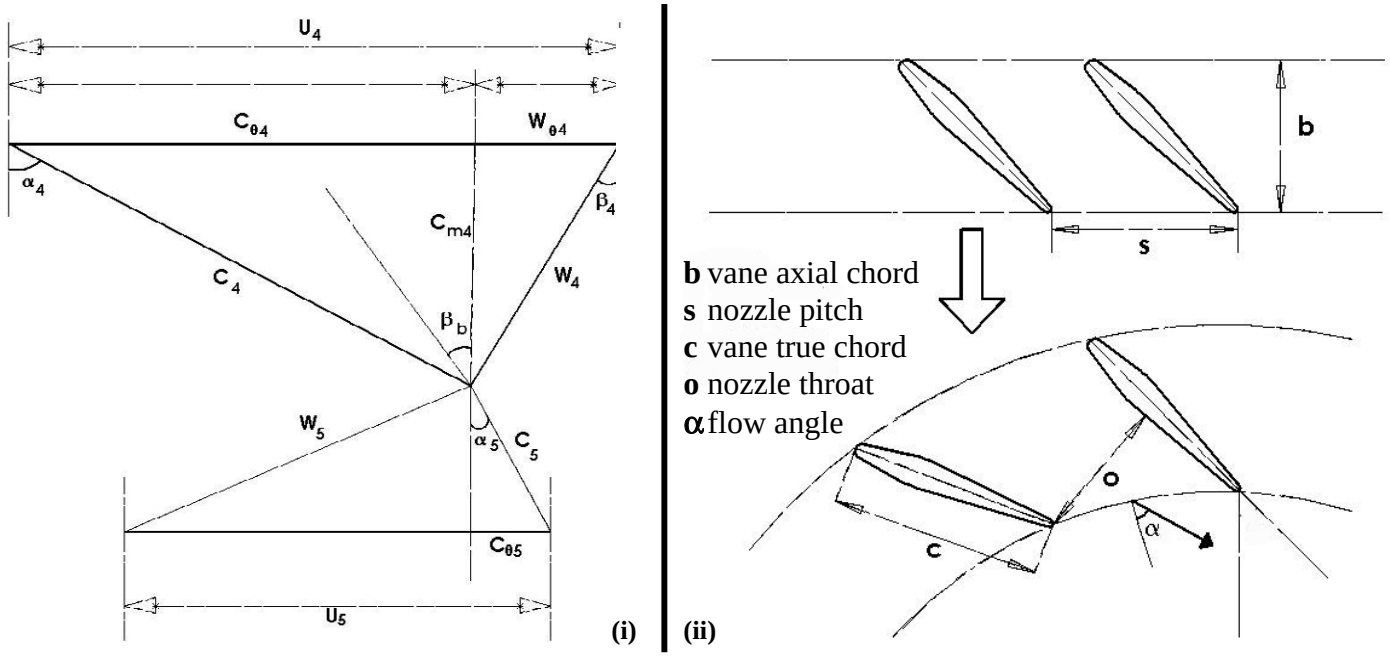

Fig. 1 (i) Velocity diagram at inlet and exit of a turbine rotor (ii) nozzle vane definitions

use of a mixed flow turbine and the new lean vane arrangement.

2. Nozzle Vane Design

This section describes the design process of the nozzle vane for a mixed flow turbine. The axial turbine blade design method was used to decide on the nozzle vane's geometries and the arrangement was consequently converted to a circumferential nozzle ring. The nozzle vane in the current study was designed un-cambered and effort was concentrated its 3-dimensional variation to fit the leading edge of a mixed flow turbine. The nozzle vane's profile was designed based on the NACA airfoil 0015. The volute used in this study was designed based on a commercial turbocharger (HOLSET H3B) with sufficient enlargement for a nozzle vane ring fitting. The volute has an inlet area over radius ratio (A/r) of 30mm and an exit flow angle of 70º.

The operating range of the vane angle was decided based on the possibility of exploring a wider range of the turbine performance and the following analysis is based on reference [8]. The velocity diagram at the inlet and exit of a turbine rotor as well as the nozzle vane definitions are given in Fig. 1. The incidence at the rotor inlet is shown in Eq. (1),

$$i = \beta_4 - \beta_b \tag{1}$$

with its optimum value is considered between -20° to -30° [8]. The rotor tip velocity, U_4 is given in Eq. (2),

$$U_4 = C_4 \sin\alpha_4 - W_4 \sin\beta_4 \tag{2}$$

Since C_{m4} and W_{m4} are the same, the inlet relative velocity is written as in Eq. (3),

$$W_4 = {C_4 \cos\alpha_4}\big/{\cos\beta_4} \tag{3}$$

Substituting Eq. (3) into (2) will eliminate W_4, as in Eq. (4),

$$U_4 = C_4(\sin\alpha_4 - \cos\alpha_4 \cdot \tan\beta_4) \tag{4}$$

For the mixed flow rotor used in this study, the blade angle, β_b is 20°. Once the inlet incidence angle is decided, the inlet relative velocity, β_4 can be calculated using Eq. (1). The rotor tip velocity can also be expressed as Eq. (5),

$$U_4 = \omega \cdot r_4, \; whereby \; \omega = {2\pi N}\big/{60} \tag{5}$$

and according to Euler's equation, assuming zero exit swirl, the power of the turbine can be approximately deduced as Eq. (6),

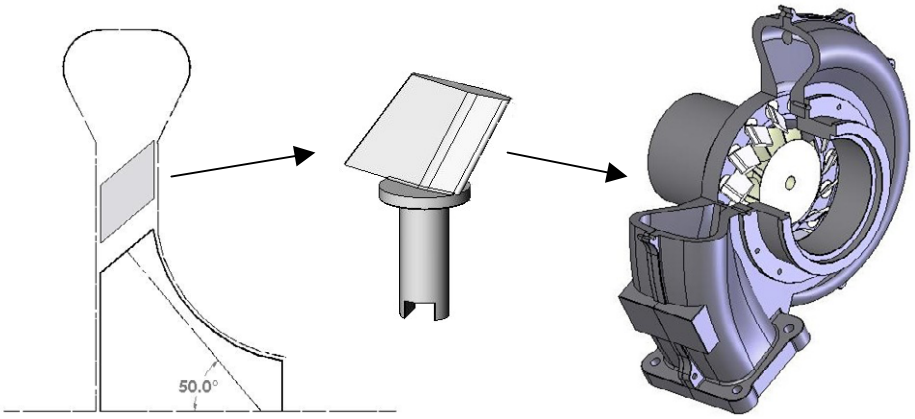

Fig. 2 Meridional projection and the lean nozzle vane assembly

$$E = \dot{m}U_4^2 \tag{6}$$

With the known range of turbine revolution speed and power absorption of the test-rig, U_4 can be calculated with Eq. (5) or (6) respectively. With the values of β_4 and U_4 known, Eq. (4) is used to calculate the value of inlet absolute velocity, C_4, for different absolute flow angles, α_4. The absolute flow velocity is then normalized and expressed as Mach number, M_4 as given in Eq. (7),

$$M_4 = \frac{C_4}{speed\ of\ sound} = \frac{C_4}{\sqrt{\gamma RT_4}} \tag{7}$$

The flow Mach number at different absolute flow angle can be calculated for a range of turbine speeds using Eq. (7). By limiting the Mach number to one, the suitable range of inlet flow angle for the power spectrum in the current application was found to be 40° to 80°. The inlet flow angle is then can be expressed as a function of the nozzle geometry [9], as in Eq. (8),

$$\alpha_4 = \alpha_3 = \cos^{-1}(o/s) \tag{8}$$

The nozzle throat, o and pitch, s are dependant on the number of nozzle vanes. Number of nozzle vanes or indirectly the blade spacing is an important factor in loss contribution and it is determined through *Zweifel's* criterion, Eq. (9),

$$\psi = 2(s/b)\cos^2\alpha_3\left|\tan\alpha_2 - \tan\alpha_3\right|, whereby \quad b = c\cos\alpha_v \tag{9}$$

The optimum pitch/chord (s/b) ratio is a compromise between friction losses and good flow guidance. The optimum tangential lift coefficient, ψ is between 0.75-0.85, which will result in the best pitch/chord compromise [8]. Since the different nozzle exit flow angle will result in different pitch/chord ratios, it was decided to match the optimum pitch/chord ratio at mid-range of the flow angles. Another compromise considered in deciding the number of nozzle vanes and the chord length for a variable geometry system is the suitable nozzle space for the capability of pivoting within the range needed. After an iterative analysis using Eq. (1)-(9), the number of nozzle vanes was decided to be 15.

The combination of a non-zero blade angle and the radial fibre, creates a degree of lean at the leading edge of a mixed flow rotor. For this reason, in order to match the nozzle vane to the leading edge of a mixed flow rotor, lean stacking was applied for the whole vane chord. Another option would have been to maintain a straight vane stacking but to have a contoured hub and shroud surface of the volute as in reference [10]. However, this will increase the difficulty in designing a reliable pivoting mechanism on an inclined surface for the variable geometry operation. The lean angle was chosen by trial and error and finally decided at 50° relative to the volute's hub surface, which in the current case is the same as the mixed flow rotor's cone angle. The resulting meridional projection of the assembly (see Fig. 2) shows good match between the nozzle vane and the rotor. Nevertheless, the lean stacking and conformal transformation leads to a non-uniform alignment between the hub-hub and the shroud-shroud surfaces of the adjacent nozzle vanes. These result in the non-uniform suction-pressure surface interactions. To resolve this, the vane profile at the shroud end was elongated to match the surface interaction at the hub end. As illustrated in the Fig. 2, this results in a small degree of sweep at the trailing edge of the nozzle vane, but without jeopardizing the mixed flow rotor inlet match. Figure 2 also shows the assembly of the volute-nozzle ring-rotor.

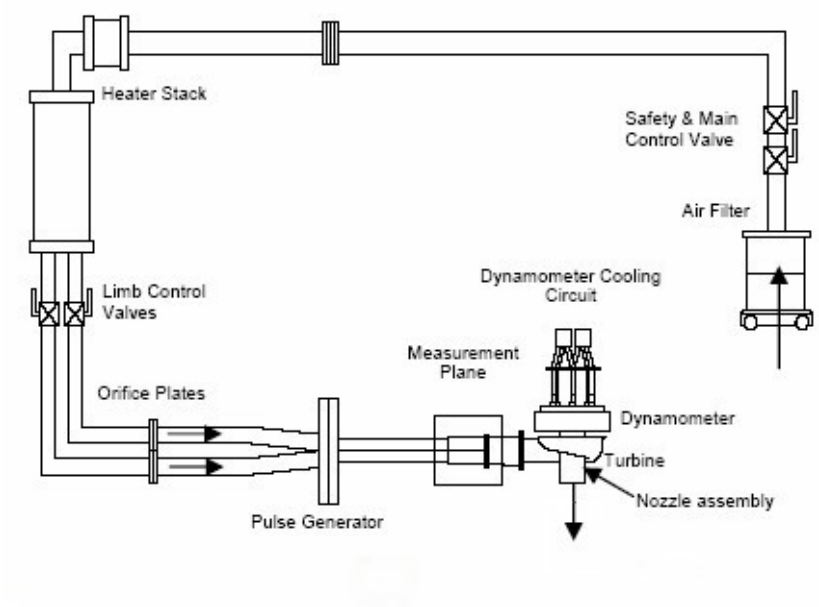

Fig. 3 Turbocharger test-rig schematic diagram

3. Experimental Setup

The experimental facility used in this study is a simulated reciprocating engine test bed for turbocharger testing. The facility has the capability of conducting steady and unsteady testing with simulated engine pulsations, as previously reported [3,4]. Furthermore, the latest instalment of eddy current dynamometer enables turbine testing within a larger velocity ratio range [11,12]. A schematic diagram of the turbine test rig is shown in Fig. 3. The test-rig is supplied by 3 screw-type compressors, capable to deliver up to 1.2 kg/s mass flow rate at a maximum pressure of 5 bar (absolute). The air flow is heated to avoid the condensation of water vapour during the expansion process within the turbine. The air pulse generator was designed to experimentally simulate the exhaust gas pulsation during unsteady testing, based on the shape of cut-outs of two counter-rotating chopper plates.

4. Results And Discussions

4.1 Vane Surface Static Pressure Survey

To evaluate the flow characteristics, the static pressure distribution on the surface of the lean nozzle vane was measured. As for comparison, similar measurement was also carried out on an equivalent straight nozzle vane. The lean and straight nozzle vanes were fabricated with rapid prototyping method and the measurement was conducted with complete assembly of the volute and nozzle vane ring, but without a rotating rotor. Instead, a dummy rotor was used with its geometry and dimension equivalent to the hub of the actual mixed flow rotor. Five static pressure tapping were drilled at mid-span from leading edge to the trailing edge, and fitted with hypodermic tubes. The static pressure tubing was extended out of the volute through the exducer. To reduce the blockage effect, the static pressure tubing was carefully packed and sealed on the volute surface.

Figure 4 shows the comparison of nozzle vane surface static pressure distribution at mid-span between the lean and the straight vanes, measured with 0.15kg/s mass flow feed into the volute, for different vane angle settings. The surface static pressure and the tapping chord length from the leading edge are normalised with the volute inlet total pressure and the true chord length of the vane respectively. The nozzle vane angles are in respect to the radial direction taken at the pivoting point on the shroud end, where increasing vane angle means the nozzle is closing. Figure 5 shows the three vane angle settings used in the testing and the measured surfaces. The suction and pressure surfaces are indicated similar to the reference [13].

At 40º vane angle, it was observed the flow is separated at the leading edge due a higher incidence. The separation effect is slightly lesser in the lean vane compared to the straight vane because the positive lean adapts better to the incoming flow. At 70º vane angle, the trailing edge region of the pressure surface forms the nozzle throat with the leading edge region of the suction surface; hence the drastic acceleration in this region, with the straight vane showing stronger convergence than the lean vane, due to the longer true span length creating higher throat area in the lean vane. For the all vane angle settings, the bigger pressure difference between the surfaces at the trailing edge indicates a possibility of higher wake loss in the lean vane. This is because the pressure at the suction surface needs to rise sharply to meet the pressure at the pressure surface. The effect is more evident at 70º vane angle setting, which can be attributed to the influence from the high velocity flow after the throat.

4.2 Steady-State Turbine Performance

The newly designed lean vanes with the volute and the pivoting mechanism were coupled to a first generation mixed flow turbine developed in the authors' institution [2]. The turbine was tested at different nozzle vane angle settings with all the necessary flow parameters measured at the measuring plane (see Fig. 3) before the volute inlet, and the turbine speed and torque were measured directly at the dynamometer. The uncertainties in the measurements are given in Tab. 1.

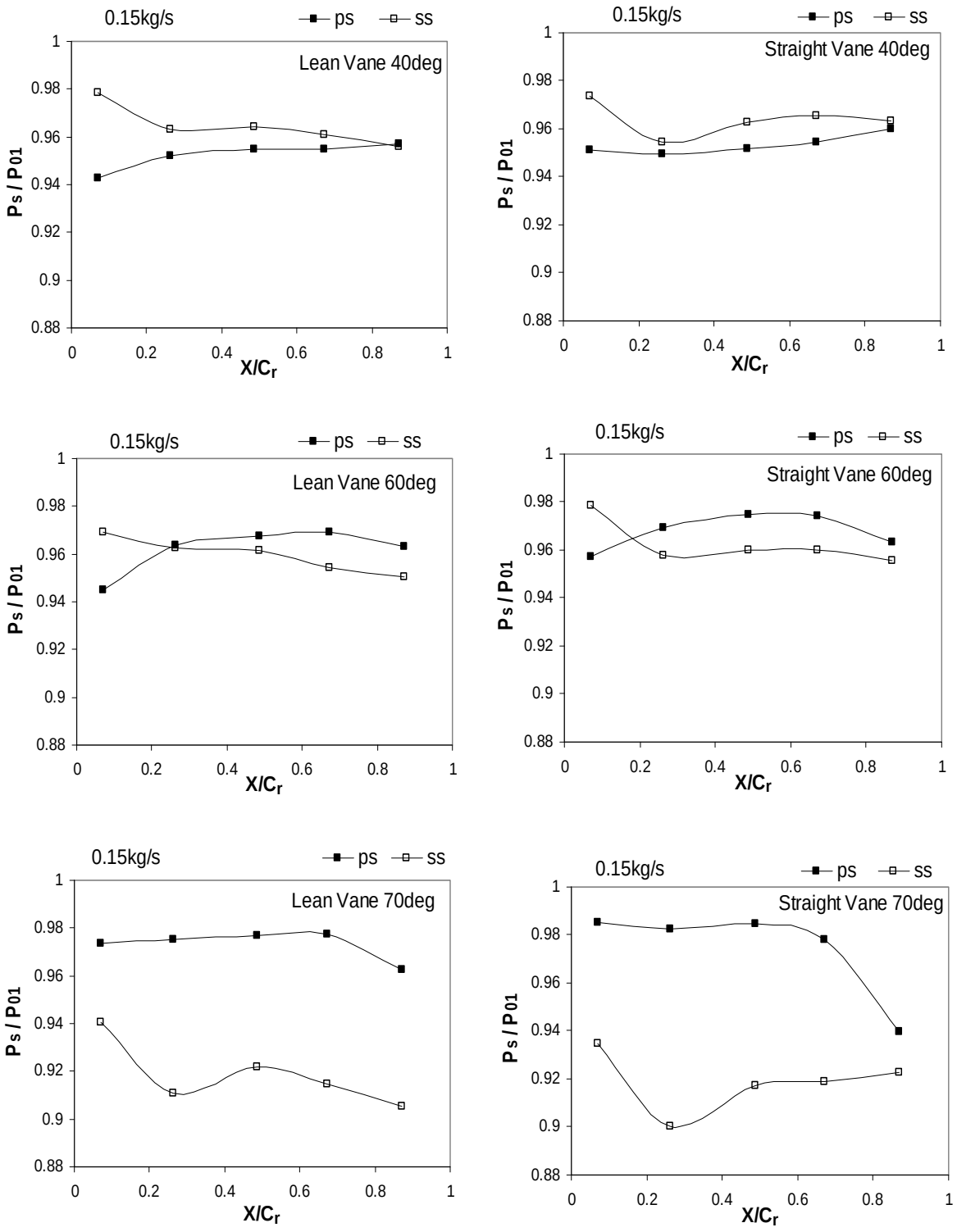

Fig. 4 Comparison of surface pressure between lean and straight nozzle vane

Table 1 Uncertainties in the measured parameters for steady and unsteady experiments

Parameters	**Root Sum Square (*RSS*) uncertainty**		
	Steady	**Unsteady (cycle averaged)**	
		40Hz	**60Hz**
Velocity Ratio, U/C_{is}	±0.2% – ±0.6%	±0.0151	±0.0154
Efficiency, η_{ts}	±1% – ±7%	±0.061	±0.063
Pressure Ratio, P_{01}/P_5	±0.1% – ±0.3%	±0.0361	±0.0298
Mass Flow Parameter, $\dot{m}\sqrt{T_{01}}/P_{01}$	±0.9% – 2%	±0.245 x 10^{-5}	±0.240 x 10^{-5}

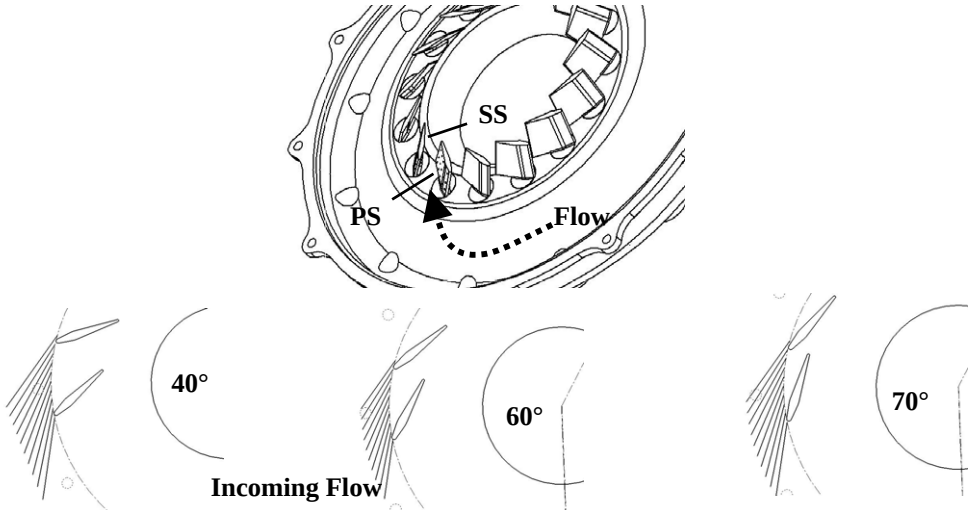

Fig. 5 Nozzle vane surface annotation and position at different vane angles

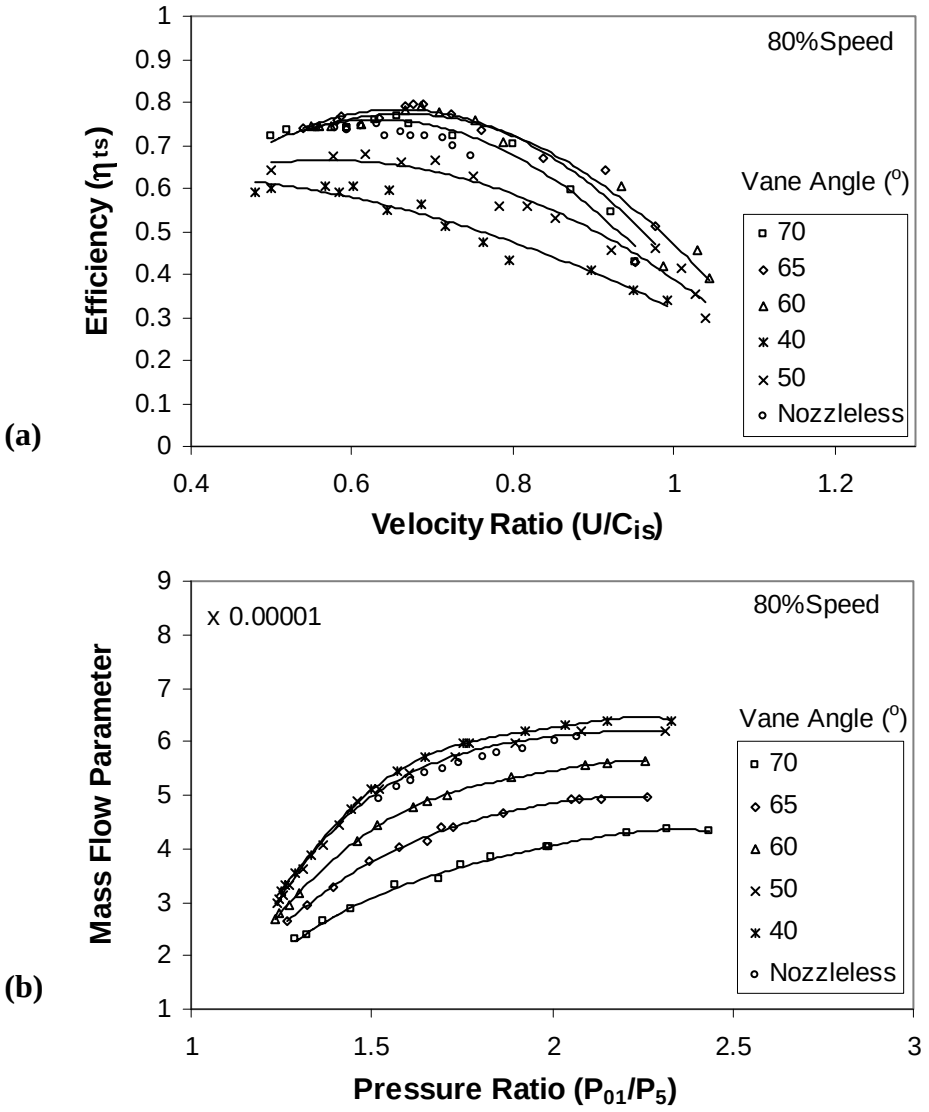

Fig. 6 Turbine performance plots at different vane angles: (a) Efficiency versus Velocity Ratio, (b) Swallowing Capacity (equivalent nozzleless result is included [4])

Table 2 Turbine Rotor Inlet Flow Conditions at Peak Efficiency for Nozzled and Nozzleless Volute

Nozzle Vane Settings	U/Cis (peak ηts)	Inlet Relative Flow Angle (β_4)	Incidence Angle β_4-β_b ,(*i*)	Loading Factor (ψ)
40°	0.57	16.4°	-3.6°	1.54
50°	0.62	15.4°	-4.6°	1.30
60°	0.68	7.4°	-12.6°	1.08
65°	0.68	9.2°	-10.8°	1.08
70°	0.66	19.5°	-0.5°	1.15
Nozzleless[4]	0.63	28.2°	8.2°	1.22

Figure 6 shows the turbine's efficiency against velocity ratio and its swallowing capacity. The figure shows results for an equivalent 80% of the design speed, which is approximately 48000rpm. The results presented are for different nozzle vane angles and comparison is shown for the same mixed flow turbine tested with a nozzleless volute [4].
The peak efficiency of the nozzleless turbine is 75% and for the vane angle of 60º, 65º and 70º, the turbine's peak efficiency shows improvement, which is 79%, 80% 77% respectively. Meanwhile, for the 40º and 50º vane angles, the peak efficiency drops to 61% and 68% respectively. This is due to the increase in separation losses in the nozzle as the vanes opens and deviate from the optimum incidence condition. Nevertheless, the 50º and 40º vane angles show higher swallowing capacity from the nozzleless turbine with approximately 2% and 8% mass flow parameter improvement respectively between the pressure ratio of 1.5 and 2.0. The swallowing capacity improvement is mainly due to a bigger volute than the nozzleless version. As for the higher vane angles, the turbine shows capability to achieve higher pressure ratio at lower mass flow parameter, for instance at the vane angle setting of 70º, pressure ratio of 1.7 is achieved with approximately 34% lower mass flow parameter compared to the nozzleless turbine. The change in the nozzle vane setting from 40º to 70º results in the turbine's efficiency to increase significantly in the first 25º and then drops slightly, meanwhile the its swallowing capacity to reduce slightly in the first 10º and then drops significantly. At 80% design speed, the vane angle setting of 65º shows the best performance at peak as well as at higher velocity ratio region.

The peak efficiency of the turbine occurs at velocity ratio range of 0.62 – 0.68 for all but 40º vane angle settings. As for the 40º vane angle setting, the peak efficiency occurs at velocity ratio of 0.57. The velocity ratio of a turbine is approximately related to the inlet absolute and relative flow angle as shown in Eq. (10),

$$\frac{U}{C_{is}} = \frac{1}{\sqrt{2}}\sqrt{1-\left(\frac{\tan\beta_4}{\tan\alpha_4}\right)} \tag{10}$$

and the turbine loading factor can be calculated as Eq. (11),

$$\psi = \frac{1}{1-\left(\frac{\tan\beta_4}{\tan\alpha_4}\right)} \tag{11}$$

Table 2 shows the calculated values based on Eq. (10) and Eq. (11), for all vane angle settings as well as the equivalent nozzleless condition. The inlet absolute flow angle, α_4 can be calculated using Eq. (8), which results in similar value as the vane angle, with maximum deviation of 7% at 70° vane angle. For the purpose of approximation, α_4 in Eq. (10) and Eq. (11) is considered equal to the vane angle, and for the nozzleless condition, it is considered equal to the volute's exit flow angle, which is 69º [4].

Based on Tab. 2, the variable nozzle positions and the nozzleless volute yield positive relative inlet flow angles at all peak efficiency conditions. The mixed flow rotor used in the study was designed with positive blade angle (see section 2), thus results in rotor incidence to vary from approximately -12.6º to -0.5º, for the nozzled settings. The 60º and 65º vane angle settings show the incidence angles closest to the optimum (see section 2) and it is reflected in the high turbine efficiency recorded. The positive incidence angle in the nozzleless version indicates the possibility of separation loss at the rotor inlet [8]. The positive relative inlet flow angles also yield a loading factor higher than unity for all the vane angle settings as well as for the nozzleless turbine, which is beneficial for high pressure turbine operation. The calculated values show the loading factor close to unity results in high turbine efficiency, as recorded for the 60º and 65º vane angle settings.

The turbine performance with the new lean nozzle vane was also compared against an equivalent straight vane. The geometry of the straight vane is same as the shroud end profile of the lean vane. Figure 7 shows the turbine's performance with lean and straight vane at an equivalent 80% design speed (48000rpm) and vane angle setting of 65º. As seen in the figure, the turbine's efficiency with both the lean and straight vane is fairly similar. It was expected that the use of lean vanes would result in higher efficiency because of the better matching to the rotor's leading edge. But the similar efficiencies suggest that there are additional losses in the lean vane compared to the straight vane which may offset any gain. One possibility of the additional losses would be the higher wetted area due to the leaning. Nevertheless, with similar efficiencies the lean nozzle vanes shows higher swallowing

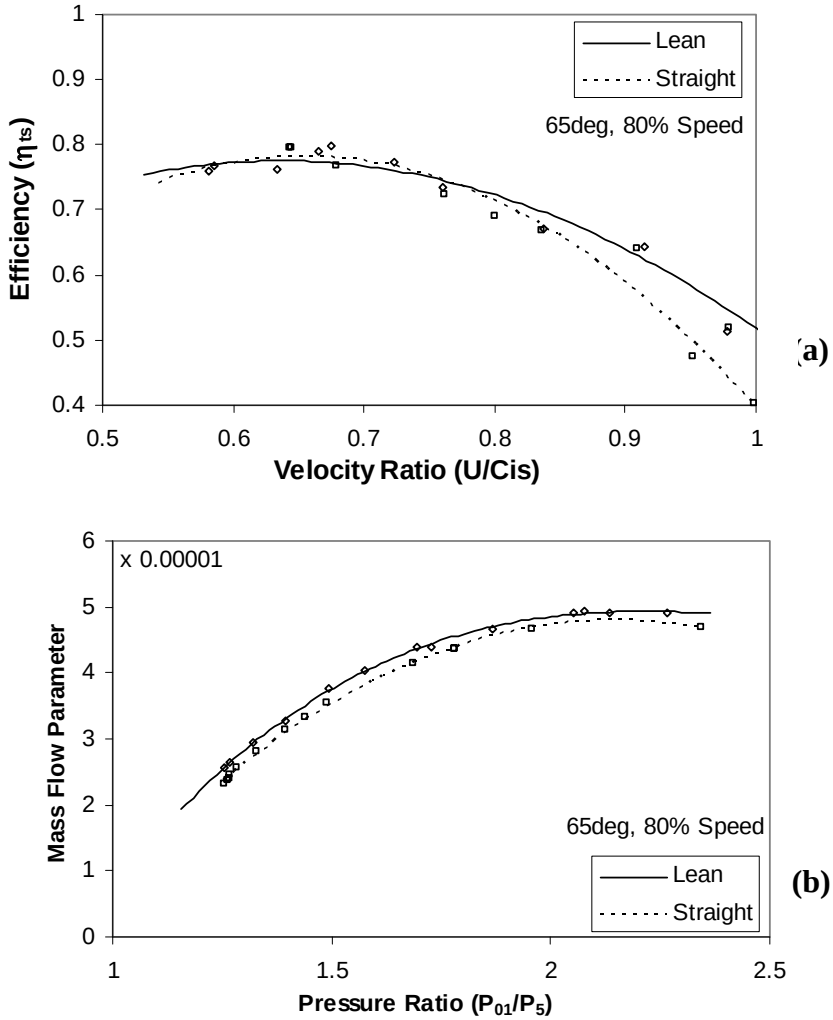

Fig. 7 Turbine performance plots with lean and straight vane: (a) Efficiency versus Velocity Ratio, (b) Swallowing Capacity

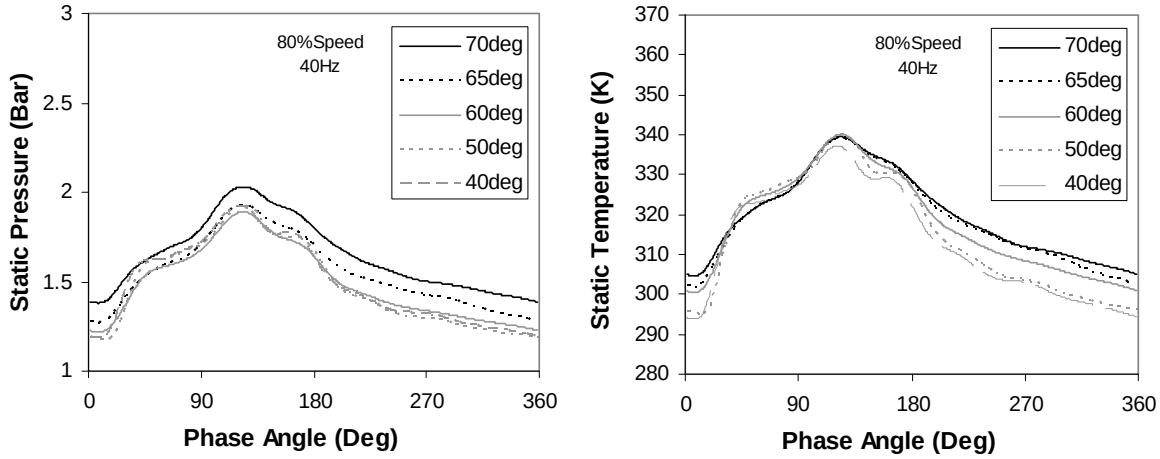

Fig. 8 Instantaneous inlet pressure and temperature with 40Hz pulsating flow at different nozzle vane angles

capacity, due to the larger nozzle area as an effect of leaning. The pressure averaged mass flow parameter of the lean nozzle vane is approximately 10% higher than the straight vane. This would be beneficial in turbocharger application, where higher swallowing capacity is often required without sacrificing the turbine efficiency.

Table 3 Unsteady cycle-isentropic power averaged and the equivalent quasi- steady efficiencies, 40Hz pulsating flow

Nozzle Vane Settings	U/Cis	Unsteady Cycle Efficiency (ηts)	Equivalent Quasi-Steady Efficiency(ηts)
40°	0.61	0.48	0.57
50°	0.61	0.49	0.64
60°	0.62	0.53	0.73
65°	0.62	0.53	0.74
70°	0.60	0.50	0.74
Nozzleless[14]	0.62	0.62	0.70

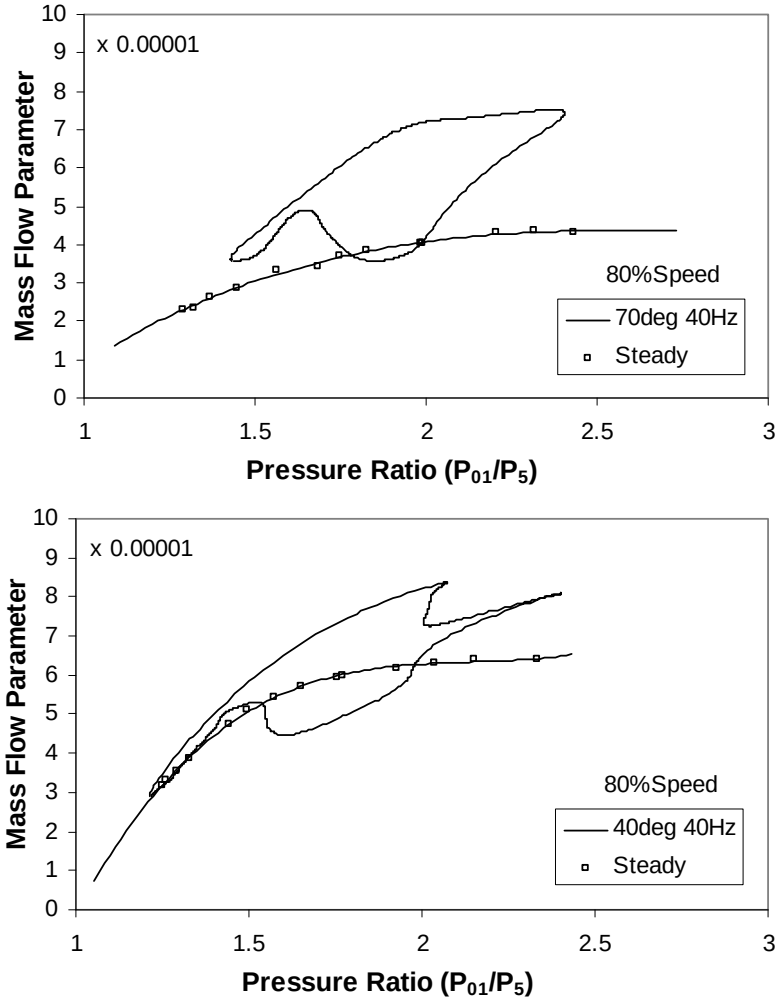

Fig. 9 Turbine's instantaneous swallowing capacity with 40Hz pulsating flow at 70° and 40° nozzle vane angles

4.3 Unsteady Turbine Performance

The performance of the turbine with lean nozzle vane was tested under pulsating flow condition for different vane angles. The pulsating frequency of the flow was 40Hz and 60Hz which approximately simulates a 3 cylinder engine running at 1600rpm and 2400rpm respectively. Testing was carried out at an average equivalent of 80% design speed (48000rpm) and flow parameters were measured instantaneously for 1800 cycles. The unsteady test condition is set up so that the average velocity ratio corresponds to its peak steady efficiency point. The detailed measuring and analysis procedures are described in Szymko et al. [12]. Figure 8 shows the measured instantaneous static pressure at the measuring plane (see Fig. 3) for one 40Hz pulse cycle. Also shown is the deduced instantaneous static temperature based on isentropic relation [12] for one pulse cycle. The pressure is observed to fluctuate from about 1.1 Bar to 1.9 Bar in most cases except for the 70° vane angle setting where a clear increase is noticed. The pulse shape in all the cases is observed to be very similar in both the pressure and temperature traces. The uncertainties in the measurements are given in Tab. 1.

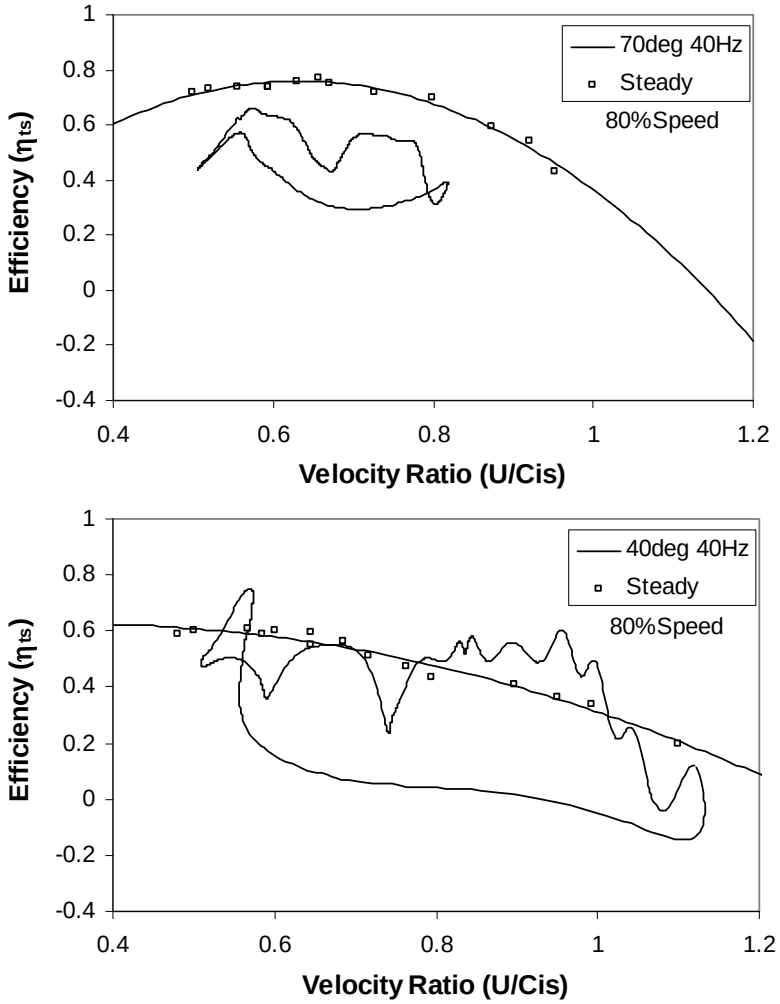

Fig. 10 Turbine's instantaneous efficiency with 40Hz pulsating flow at 70° and 40° nozzle vane angles

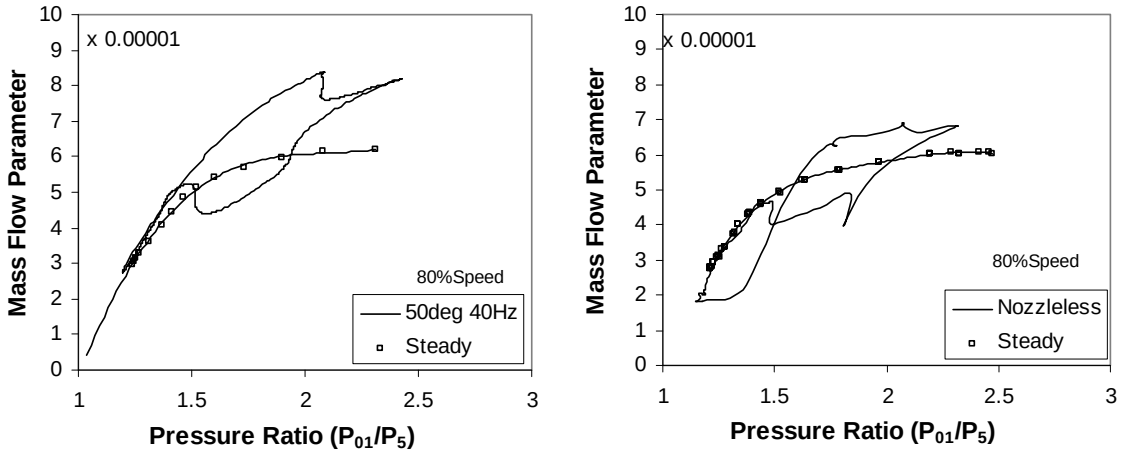

Fig. 11 Turbine's instantaneous swallowing capacity with 40Hz pulsating flow at 50° nozzle vane angle and an equivalent nozzleless unit [14]

Figure 9 illustrates the turbine's instantaneous swallowing capacity at 40Hz pulse cycle for 70° and 40° vane angle settings. Similarly, the turbine's instantaneous efficiency for the settings is shown in Fig. 10. The instantaneous efficiency is calculated based on the isentropic condition measured at the measuring plane (upstream of the volute inlet, Fig. 3) and the actual power measured at the dynamometer end. The two traces are matched by applying a phase shifting with the sum of bulk and sonic velocities [12]. It should be noted here that the instantaneous efficiency refers to the stage from the measuring plane to the turbine

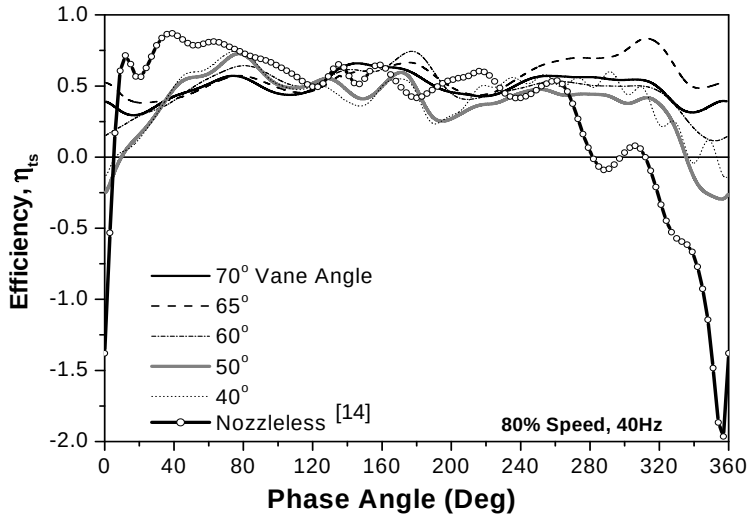

Fig. 12 Turbine's instantaneous efficiency for one complete pulse cycle

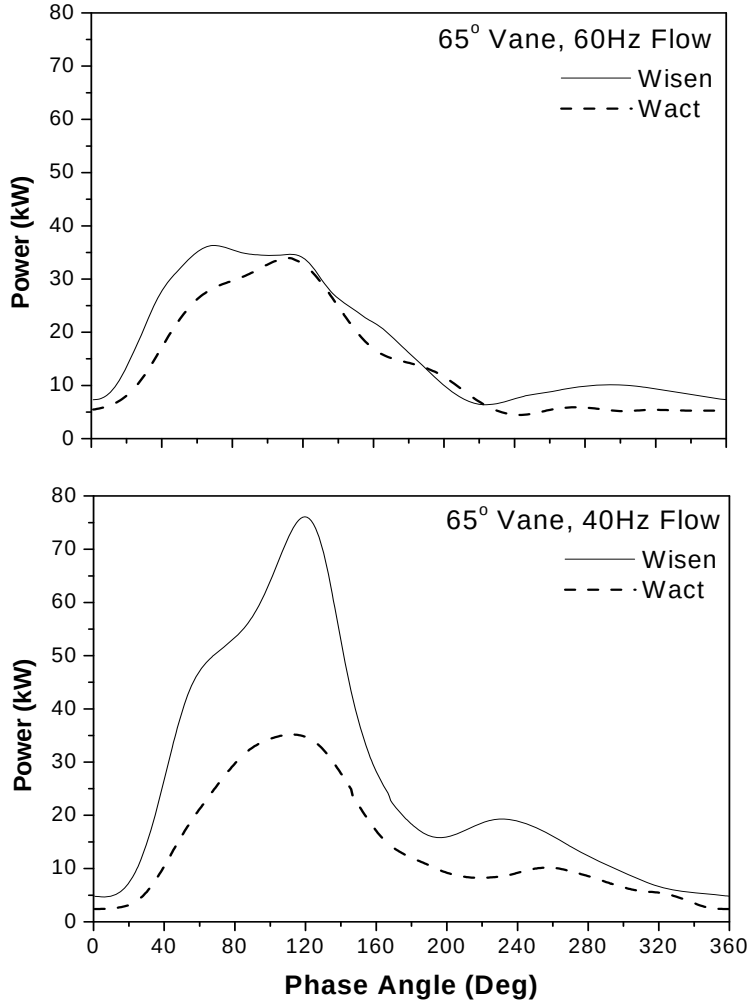

Fig. 13 Turbine's actual and isentropic power at 65° vane angle, with 40Hz and 60Hz pulsating flow

exit. It is observed that the turbine's performance curves exhibit hysteresis loop, but with significant deviation from the quasi-steady condition. The deviation is substantial in the 70° vane angle setting, but reduces as the nozzle vanes open to 40°. The velocity ratio range covered by the turbine in a pulse cycle is found to be small and concentrated at the lower region at close nozzle position. The range gradually increases as the nozzle opens to 40° vane angle setting.

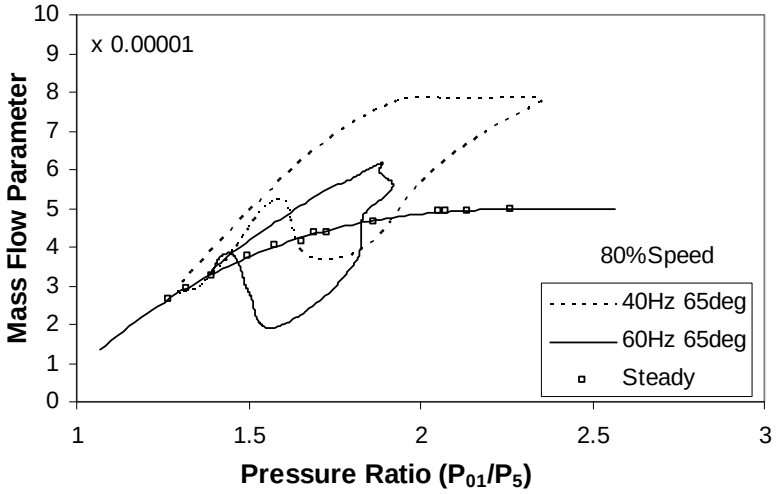

Fig. 14 Turbine's instantaneous swallowing capacity at 65° vane angle, with 40Hz and 60Hz pulsating flow

Figure 11 shows the swallowing capacity of an equivalent nozzleless turbine during a 40Hz pulse cycle [14]. Also given in the figure is the similar curve for the 50° vane angle setting, where the VG turbine's steady swallowing capacity equivalent to the nozzleless unit. It can be seen that the hystherisis loop is shifted slightly upwards in the VG turbine but the pressure ratio range covered by the turbine is similar. Comparing the nozzleless curve with the results for 70° vane angle settings (Fig. 9) shows a substantial difference, especially the deviation from quasi steady line. It is suggested the existence of a nozzle ring creates two volumes before the rotor, one in the volute and one in the nozzle, where the filling-emptying characteristics of both are different and changes with nozzle opening. This consequently results in the different unsteady behaviour measured in a VG turbine compared to a nozzleless unit.

During pulsating flow the turbine volute experiences continuous filling and emptying and in the 70° vane angle setting, due to the high blockage of the nozzles, the emptying of the volute is delayed before the filling occurs in the consequent pulse. This creates a back pressure and eventually mass accumulation in the volute. It is suggested that the slow emptying process of the volute may have resulted in the higher mass flow rate measurement, which in reality does not reflect the true instantaneous mass impacting momentum on the rotor. This eventually leads to the lower efficiency calculation for the 70° vane angle setting. The high mass flow rate reading is evident in the Fig. 9 and it is also noticed that the turbine experiences choking at high pressure ratio region in the 70° vane angle setting. Similar choking behaviour was also observed for the 65° and 60° vane angle settings. On the other hand, at 40° vane angle setting the turbine did not experience choking and loops more closely to the quasi-steady curve. Table 3 shows the cycle averaged efficiencies and velocity ratios of the turbine at different nozzle vane angle settings as well as the nozzleless condition, for 40Hz pulsating flow. These parameters are averaged using isentropic power average method, which is described in reference [12]. The equivalent quasi-steady efficiencies calculated, where at each instance of time the instantaneous velocity ratio is used to read the steady efficiency and consequently power averaged over a cycle. It is noticed at all nozzle vane angle settings the cycle averaged turbine efficiency are significantly lower than the equivalent quasi-steady value and the nozzleless condition. At 70° vane angle, the unsteady cycle efficiency is about 32% lower than the equivalent quasi-steady efficiency and it gradually improves to about 17% at 40° vane angle. The cycle averaged efficiency shows the turbine performs better at 60° and 65°, which is similar to the steady state findings.

Figure 12 shows the turbine efficiency variation plotted for a 40Hz pulse cycle for all the nozzle vane angle settings as well as the nozzleless condition [14]. It can be noticed that the nozzleless turbine exhibit negative efficiency at the beginning and end of the cycle. The negative efficiency can be explained as the consequence of turbine rotor impacting momentum on the flow at lower pressure ratio conditions [12]. As for the nozzled settings, the turbine did not exhibit negative efficiency at 70°, 65° and 60° vane angle settings. This is due to the nozzle constantly providing sufficient flow momentum to the rotor during the pulse cycle. But at 40° and 50° vane angle settings, the turbine gradually exhibits negative efficiency, as the opening of the nozzle reduces the momentum of the flow in low pressure ratio region. It is also noticed that during the first 120° crank angles, where most of the isentropic power concentrated in the pulse, nozzleless turbine exhibits better efficiency than the nozzled turbine. For the rest of the cycle, the efficiency of the nozzleless turbine drops in comparison to the nozzled turbine. Another interesting observation is that at 65° vane angle setting, the turbine shows good efficiency towards the end of the cycle, which suggests better energy extraction from the lower pressure region of the pulse. However, it should be noted that the calculated instantaneous efficiency is sensitive to the method of phase shifting and the influence of filling-emptying or wave action in the volume. Thus careful examination of the flow condition at each instance in time is required before conclusive judgement can be made of the turbine's unsteady instanatenous efficiency.

Figure 13 shows the turbine's isentropic and actual power comparison for 40Hz and 60Hz pulsating flow conditions with vane angle setting of 65º. The cycle averaged actual power of the turbine is 14.1 kW and 14.3 kW for 40Hz and 60 Hz pulsating flow respectively. The turbine's actual power over a cycle period as well as its pattern is approximately similar between both the flow frequencies, but the isentropic condition at the inlet of the turbine is significantly different. This is mainly due to the faster duty cycle of the pulse generator in 60Hz condition, which results in a lesser energy per cycle to achieve an equivalent output to the

40Hz condition. This eventually leads to a better emptying effect in the volute before the next cycle of the filling occurs. Figure 14 shows the turbine's swallowing capacity for both the frequencies. The curve in the 60Hz condition is found to loop around the steady line but with smaller pressure ratio range, but in the 40Hz condition the curve is shifted upwards. Furthermore, choking of the turbine was not observed in the 60Hz pulsating flow condition. The isentropic power averaged velocity ratio and efficiency of the turbine at 60Hz pulsating flow is 0.66 and 80% respectively (values for the 40Hz is shown in Tab. 3). The equivalent quasi steady efficiency is 76.3%.

5. Conclusions

A new nozzle vane ring has been designed to match the 3-dimensional feature of the leading edge of a mixed flow rotor. It was found that for nozzle vanes in a volute, the suction surface pressure is higher than the pressure surface, especially at closer nozzle positions. This is due to the dominant effect of the flow in the volute, at the upstream and downstream of the nozzle vane, compared to the adjacent vane interaction effect.

The VG mixed flow turbine performance was tested at different vane angle settings, under steady and unsteady conditions. The VG mixed flow turbine shows efficiencies at nozzle vane angle of 60º, 65º and 70º higher than the nozzleless turbine for much of the velocity ratio range, with highest peak efficiency of 80% obtained at 65º vane angle. The swallowing capacity of the VG turbine at fully opened condition (40º vane angle) is up to 8% higher than the nozzleless turbine. The VG turbine is capable of achieving high pressure ratio at lower inlet mass flow, which demonstrates its benefit in adapting to off-peak conditions during the turbine operation. Performance comparison with an equivalent straight vane design shows the higher swallowing capacity of the lean vane with similar efficiency at almost all pressure ratio conditions.

The VG turbine's unsteady performance shows substantial deviation from the equivalent quasi-steady assumption at 40Hz pulsating flow, especially at close nozzle positions (60º, 65º, 70º), as much as 33% at 70º vane angle setting. This is due to the high blockage in the nozzle which consequently leads to choking and delaying the volute emptying, before the next cycle of filling. The existence of a nozzle ring in effect creates two volumes in the stator (volute and nozzle passage), where its filling-emptying characteristics are different. The effect of both these volumes contributes to the significant difference observed compared to a nozzleless version. At 60Hz pulsating flow, the faster duty cycle of the pulse generator creates lower energy in a cycle which leads to better filling-emptying effect in the volume. This is reflected in the high cycle averaged efficiency recorded for this condition.

Acknowledgement

The authors would wish to thank the Engineering and Physical Sciences Research Council (E.P.S.R.C) and University Technology Malaysia for their financial as well as Mr. Harminder Flora and Mr. Nick Sharp (Holset Engineering) for their technical support.

Nomenclature

C	Absolute flow velocity, m/s
c	Vane true chord, m
C_{is}	Isentropic velocity, m/s
E	Turbine Power, W
M	Mach number
R	Universal gas constant, J/kg.K
T	Temperature, K
P	Pressure, Bar
U	Rotor velocity, m/s
W	Relative flow velocity, m/s
b	Vane axial chord, m
o	Nozzle throat width, m
r	Radius, m
s	Nozzle pitch, m
$\dot{m}$	Mass flow rate, kg/s
α	Absolute flow angle, deg
β	Relative flow angle, deg
γ	Specific heat ratio
ψ	Tangential lift coefficient
η	Efficiency
$\dot{m}\sqrt{T_{01}}/P_{01}$	Mass Flow Parameter

Subscript

b	Rotor blade
v	Nozzle vane
0	Total condition
1	Turbine inlet condition
2	Nozzle inlet condition
3	Nozzle exit condition
4	Rotor inlet condition
5	Turbine exit condition (atm)
θ	Tangential component
ts	Total to static

References

[1] Baines, N.C., Wallace, F.J. and Whitfield, A., 1979, "Computer Aided Design of Mixed Flow Turbines for Turbochargers," Transaction ASME, Vol. 101, pp. 440-449.

[2] Abidat, M., Chen, H., Baines, N.C., 1992, "Design of a Highly Loaded Mixed Flow Turbine," Proceedings Instn. Of Mech. Engrs., Vol. 206.

[3] Arcoumanis, C., Hakeem, I., Khezzar, L. and Martinez-Botas, R.F., 1995, "Performance of a Mixed Flow Turbocharger Turbine Under Pulsating Flow Conditions," Transaction ASME, paper 95-GT-210.

[4] Karamanis, N., Martinez-Botas, R.F., 2002, "Mixed Flow Turbines for Automotive Turbochargers: Steady and unsteady Performance," IMechE Int. J. Engine Research, Vol. 3(3), pp. 127-138.

[5] Baets, J., Bernard, O., Gamp, T., and Zehnder, M., 1998, "Design and Performance of ABB Turbocharger TPS57 with Variable Turbine Geometry," 6th Int. Conf. on Turbochargers and Turbocharging, Proc. of the IMechE, paper C554/017/98, pp. 315-325.

[6] Winterbone D.E., Nikpour B. and Alexander, G.I., 1990, "Measurement of the Performance of a Radial Inflow Turbine in Steady and Unsteady Flow," Proc. IMechE, paper C405/015, pp. 153-162.

[7] Kosuge, H., Yamanaka, N., Ariga, I., and Watanabe, I., 1976, "Performance of radial flow turbines under pulsating flow conditions," Trans. of the ASME, J. of Engineering for Power, Vol. 98, pp. 53-59.

[8] Japikse, D. and Baines, N.C., 1994, Introduction to Turbomachinery, Concept ETI Inc., USA and Oxford University Press, Oxford.

[9] Hiett, G.F. and Johnston, I.H., 1963, "Experiments Concerning the Aerodynamic Performance in Inward Radial Flow Turbines," Proc. of the IMechE, 178, Part 3I(II), pp. 28-42.

[10] Kirtley, K.R., Beach, T.A., Rogo,C., 1993, "Aeroloads and Secondary Flows in a Transonic Mixed Flow Turbine Stage," Trans. of ASME, 115, pp. 590-601.

[11] Szymko, S., Martinez-Botas, R.F., Pullen, K. R., McGlashan, N.R. and Chen, H., 2002, "A High-Speed, Permanent Magnet Eddy-Current Dynamometer for Turbocharger Research," 7th Int. Conf. on Turbochargers and Turbocharging, Proc. of the IMechE, paper C602-026.

[12] Szymko, S., Martinez-Botas, R.F. and Pullen, K.R., 2005, "Experimental Evaluation of Turbocharger Turbine Performance under Pulsating Flow Conditions," Proc. of ASME Turbo Expo, paper GT 2005-68878.

[13] Spence, S.W.T., O'Neill, J.W. and Cunningham, G., 2006, "An Investigation of the Flowfield Through a Variable Geometry Turbine Stator with Vane Endwall Clearance," Proc. of the IMechE, Vol 220, Part A: J. Power and Energy, pp. 899-910.

[14] Szymko, S., 2006, "The Development of an Eddy Current Dynamometer for Evaluation of Steady and Pulsating Turbocharger Turbine Performance," PhD Thesis, Department of Mechanical Engineering, Imperial College London, UK.